47th AIAA Aerospace Sciences Meeting Including The New Horizons Forum and Aerospace Exposition
5 - 8 January 2009, Orlando, Florida

AIAA 2009-941

An evaluation of shock-capturing methods on a hypersonic boundary layer receptivity problem

Syed F. Rehman,* Jeff D. Eldredge,† Xiaolin Zhong,‡ and John Kim.§
Mechanical & Aerospace Engineering Department, University of California, Los Angeles
Los Angeles, CA, 90095, USA

Understanding of transition of hypersonic boundary layers is critical for future development of re-entry vehicles. The receptivity of such a boundary layer to external flow disturbances is not well understood, particularly when the surface has finite-sized roughness. In this work, we explore the use of shock capturing for study of hypersonic boundary layer receptivity. In such problems, the interaction of the low-amplitude disturbances with shock structures may not be properly accounted for due to the localized dissipation inherent in the method. Previously-developed previously-developed WENO-based third- and fifth order shock capturing methods are applied to a receptivity problem, the Mach 4.5 flow past a flat plate with a sharp leading edge. This problem has been studied previously with a high-order shock fitting scheme. The shock-fitted solution is used to evaluate shock capturing schemes in terms of accuracy, efficiency and stability. Also, the significance of the leading edge singularity will be studied, which was not possible with a shock fitting method.

I. Introduction

The transition to turbulence from a laminar boundary layer in supersonic and hypersonic flow is key in the future development of space vehicles. Physically, a turbulent flow applies greater shear and thermal stresses on a vehicles than a laminar flow, hence an accurate prediction to turbulence plays a critical role in the structural and thermal design of these vehicles. Transition to turbulence generally occurs due to the nonlinear interaction between the boundary layer and freestream disturbances.[5,6,18,20] Now, if the freestream disturbances are small in amplitude then the transition process starts near the leading edge of the body with the receptivity process. This process is critical since it consists of the initial exchange of energy between the freestream disturbances and the boundary layer modes, for example, the Tollmien-Schlichting (T-S) modes.[19,50] The receptivity then leads to a transient stage where the boundary layer modes exhibit a linear eigenmode growth. The nonlinear interaction between several of these amplitude increasing boundary layer modes leads to turbulence. Other forms of transitions to turbulence are also possible. For example, a transition known as a "bypass transition" occurs when the amplitude of the freestream disturbances is relatively large. In a bypass transition the linear growth of boundary layer modes is not present. A high altitude atmospheric re-entry flight generally undergoes small amplitude disturbances, hence the process of receptivity becomes crucial in understanding transition.

*Graduate Student, email: chronolz@seas.ucla.edu. Student Member, AIAA.
†Assistant Professor, email: eldredge@seas.ucla.edu. Member, AIAA.
‡Professor, Associate Member, AIAA.
§Professor, Member, AIAA.

A popular transition prediction approach is the e^N method, however, it lacks the accountability of the freestream disturbances in the process of transition, i.e. the process of receptivity. Receptivity for incompressible flow has been under extensive study over the last few decades.[49] However, studies of compressible flow receptivity have shown that the process of receptivity for supersonic and hypersonic flows differs fundamentally when compared to receptivity of subsonic and weakly supersonic flows.[21,22,41,43] The process of receptivity consists of the interaction of freestream disturbances with the boundary layer modes, which have been well characterized by Mack,[37] referred to now as Mack modes. Various theoretical studies have observed the significance of the receptivity process near the leading-edge and the dependence of boundary layer mode excitation on diffraction, diffusion and the incident angle of the incoming freestream disturbances.[17,34,37,39–43] Experimental studies have also elaborated on the significant dependence of the transition location on the initial freestream disturbances, i.e. receptivity.[33,35,36,44,45,48]

Computational studies using direct numerical simulation (DNS) have also been conducted in understanding the process of receptivity.[15,16] Using a fifth order shock fitting scheme, Zhong[32] studied the receptivity of a hypersonic boundary layer over a parabola and concluded that acoustic disturbances dominate in the transfer of energy to the boundary layer modes over vorticity and entropy waves. A Mach 4.5 DNS over a flat-plate was performed by Ma & Zhong.[21,22] They observed the generation of a family of stable modes in conjunction with the first two dominant Mack modes in the process of receptivity. The stable modes were observed to act as a medium in the transfer of energy between the freestream disturbances and the unstable Mack modes. Egorov *et al.*, simulated a supersonic boundary layer using a TVD scheme and their result agreed well with LST.[8]

The receptivity of a compressible boundary layer over a flat plate under supersonic and hypersonic conditions involves the propagation of very small wave disturbances, hence a relatively high order spatial scheme is required to properly capture these physical phenomenon. The analysis is further complicated by the presence of a bow shock, for example, generated near the leading edge of the flat plate. It is well known that any wave, whether it is an acoustic wave, an entropy wave or a vorticity wave interacting with a shock always generates all three of these wave in the downstream region.[7] In the flow over a flat plate the freestream disturbances first pass through the shock. These waves then diffract near the leading edge and also reflect off the flat-plate boundary and propagate back to the shock and go through more reflections there. Hence, the receptivity of a relatively simple geometry is made considerably more complicated. Ma & Zhong[21,22] conducted a DNS of this problem using a fifth order shock fitting scheme.[23] The shock fitting algorithm gives the flexibility of using a relatively high order spatial scheme needed for resolving small amplitude wave propagation with a presence of a shock at a boundary of the computational domain.

Even with these advantages, the shock fitting method is limited to only resolving simple shock structures, for example, shocks over a blunt body. The shock fitting method fails to resolve the leading edge singularity and other complicated shock structures, which maybe present in the flow for example due to an isolated surface roughness.

A. Previous approaches to shock capturing methods

To overcome some of these limitations of shock fitting, various high order shock capturing algorithms are available. Shu & Osher[24] developed a high order cell based Essentially Non Oscillatory (ENO) scheme which overcame low order limitations of previous shock capturing schemes such as various time varying diminishing (TVD) schemes. Jaing & Shu[31] further extended the cell based ENO scheme to a node based Weighted ENO scheme (WENO). They were also able to modify the smoothness indicators to acquire the nominal order of accuracy in the smooth regions. However, shock capturing schemes have their own drawbacks. Perhaps the biggest disadvantage is that

any unsteady solution propagating through the shock reduces to first order accuracy.[46] Another disadvantage is that a shock capturing scheme is computationally expensive relative to conventional finite difference schemes. The increased expense comes from the automated determination of high-gradient zones and reduction of algorithm accuracy near these zones in-order to keep the solution essentially oscillation free. To reduce the dissipative nature of the WENO scheme, Martin & Taylor *et al.*[28] have performed optimization of the underlying differencing operator in wavenumber space. Instead of using an upwind stencil, they used a symmetric stencil with a free stability parameter to reduce dissipation while maintaining the high order of accuracy.

To reduce the computational expense of WENO, various researchers have adapted hybrid approaches where the WENO algorithm is applied primarily near discontinuities. For example, Pirozzoli[25] combined a conservative upwind compact finite difference with a conservative WENO method. However, there was a slight problem with abrupt switching between the two algorithms which was improved by Ren *et al.*[27] Hill & Pullin[26] used a central difference scheme in the smooth regions to further reduce dissipation. Taylor *et al.*[29] decided not to use two different schemes between smooth and discontinuous regions. Instead two rate limiters were introduced, which limit the activation of the WENO weights to discontinuous zones. It was noted earlier that any solution passing through the shock reduces in accuracy to first order. Casper[46] was able to develop a sub cell refinement procedure for the shock zone in order to maintain the nominal order of accuracy of the method for a 1D problem. However, drawbacks were noted on the added expense required and further complication of extending the procedure to multi-dimensional problems. A multi-dimensional hybrid WENO with sub-cell refinement has also been developed.[30]

B. Scope of this work

Keeping the above questions in mind, the purpose of this work is to examine the accuracy of shock capturing when applied to hypersonic boundary layer receptivity. This assessment will be made on the benchmark problem of a Mach 4.5 flow past a flat plate, previously computed by Ma & Zhong using a higher order shock fitting method.[21] The schemes of interest include the third and fifth order conventional WENO scheme mentioned earlier.[31] One objective here is to evaluate shock capturing schemes in terms of accuracy, stability and efficiency with a conventional shock fitting finite difference scheme on the complicated physics of receptivity. Another objective here is to determine whether the leading edge, which was previously excluded, plays any significant role in the problem of receptivity. This benchmark of the selected shock capturing methods will help asses their effectiveness and robustness for the hypersonic receptivity simulations. This study will also test some of its limitations, in terms of dissipation and computational expense, perhaps shedding critical insight on possible algorithm refinements.

A successful receptivity study will give confidence in these schemes in accessing new and more complicated receptivity studies such as receptivity of a hypersonic boundary layer with an isolated or distributed surface roughness elements of finite heights.

II. Governing equations

The conservative form of the compressible Navier-Stokes equations in curvilinear coordinates is used to obtain solution to the numerical experiments.[3] The vector representation of these equations in two-dimensional Cartesian coordinates, to avoid excessive cluttering, is given by

$$\begin{bmatrix} \rho \\ \rho u \\ \rho v \\ e \end{bmatrix}_t + \begin{bmatrix} \rho u \\ \rho u^2 + p - \tau_{xx} \\ \rho uv - \tau_{xy} \\ (e+p)u - u\tau_{xx} - v\tau_{xy} + q_x \end{bmatrix}_x + \begin{bmatrix} \rho v \\ \rho uv - \tau_{xy} \\ \rho v^2 + p - \tau_{yy} \\ (e+p)v - u\tau_{xy} - v\tau_{yy} + q_y \end{bmatrix}_y = 0 \tag{1}$$

or in a general conservation form

$$U_t + f_x + g_y = 0 \tag{2}$$

where, in both equation (1) and (2), the subscripts x and y denote their respective derivatives in spatial directions of x and y, while the subscript t denotes a derivative in time.

In equation (1) e, τ_{ij} and q_i represent the total energy, viscous stress tensor and the heat flux, respectively, given by

$$e = \frac{p}{\gamma - 1} + \frac{1}{2}\rho\left(u^2 + v^2\right), \tag{3}$$

$$\tau_{ij} = \mu\left(\frac{\partial u_i}{\partial x_j} + \frac{\partial u_j}{\partial x_i}\right) - \frac{2}{3}\mu\frac{\partial u_k}{\partial x_k}\delta_{ij}, \tag{4}$$

$$q_i = -\kappa\frac{\partial T}{\partial x_i}. \tag{5}$$

Equations (4) and (5) include μ and κ, the dynamic viscosity and the thermal conductivity, respectively. The viscosity is computed using Sutherland's law, while the thermal conductivity is related to μ via the Prandtl number; the Prandtl number is taken to be $Pr = \mu c_p/\kappa = 0.72$, the Prandtl number of air. Last, the state equation for thermally and calorically perfect gas is used to close the system of equations,

$$p = \rho RT. \tag{6}$$

III. Numerical Method

The method of lines is used to construct a system of semi-discrete ordinary differential equations from the system of partial differential equations. All numerical experiments conducted in this paper use Roe average flux splitting.[4] This work is interested in numerical experiments of hypersonic and supersonic flow problems where complex shock structures may be present. Hence, inviscid fluxes are reconstructed with a shock capturing algorithm. Furthermore, the shock capturing algorithm must be based on a higher order method such that it is able to propagate low-amplitude waves and transmit them through a shock with reasonable grid resolution and low numerical dissipation. The WENO method is used in all of the numerical experiments in this paper.[31]

A WENO reconstruction of a flux with $2r-1$ order accuracy uses a stencil with $2r-1$ points. This stencil consists of smaller r substencils. Associated with each substencil is a lower order flux reconstructions, a smoothness indicator, and a nonlinear WENO weight. The lower order substencil flux reconstructions are multiplied by their respective weights and then summed over the entire stencil to reconstruct the higher order flux. The smoothness indicators determine whether a WENO weight is nearly zero in non-smooth regions or nearly a constant, C_l, in smooth regions. When

a substencil is in a discontinuous region its WENO weight approaches zero, effectively negating the associated substencil flux. When the substencil is in a smooth region its weight approaches the constant, C_l, retaining the nominal accuracy of the substencil flux there. There are many variations of WENO. In the present work Jiang and Shu's WENO scheme is used in all numerical experiments.[31] A third order TVD Runge-Kutta scheme is selected to integrated the semi-discrete equation in time.[31]

IV. Frequency Analysis

Before proceeding to the benchmark problem of receptivity over a flat plate, it is important to understand how the nonlinear WENO scheme behaves for a simple wave propagation. This analysis will provide guidance on the required grid resolution for resolving the flow structures associated with the linear problem of receptivity

The current analysis follows that of Pirozzoli,[2] where a modified wavenumber is obtained numerically for nonlinear shock capturing schemes. Consider the following linear wave equation

$$U_t + f_x = 0, \quad U(x,0) = U_0(x) \quad -\infty < x < +\infty \tag{7}$$

where

$$f(U) = aU, \quad a = \text{const.} > 0 \tag{8}$$

and the function is initially sinusoidal,

$$U_0(x) = \hat{U}_0 e^{ikx}, \tag{9}$$

where k is a wavenumber. The exact solution to the linear wave equation for this initial condition is given by

$$U(x,0) = \hat{U}_0 e^{ik(x-at)}. \tag{10}$$

Now, suppose the problem is solved on a periodic grid with uniform resolution $x_j = j\Delta x$. In discrete form equation (7) becomes

$$\frac{dU_j}{dt} = -\frac{a}{\Delta x}\sum_{l=-r}^{r} a_l U_{j+l}, \quad U_j(0) = \hat{U}_0 e^{ijk\Delta x} \tag{11}$$

Note, for a linear differencing equation (11) has a well-known exact solution

$$U_j(t) = \hat{U}(t) e^{ijk\Delta x}, \tag{12}$$

where the complex time dependent amplitude is expressed as

$$\hat{U}(t) = \hat{U}_0 e^{-i(at/\Delta x)\Phi(k\Delta x)} \tag{13}$$

and $k\Delta x$ is the reduced wavenumber and Φ is the modified wavenumber, which ideally is $\Phi(k\Delta x) = k\Delta x$.[1]

For a nonlinear scheme such as WENO, such an exact solution is not possible. To obtain the modified wavenumber numerically, Pirozzoli[2] proposed to first numerically compute a forward propagating wave advanced to a small time t_s, $U_j(t_s)$, then compute its discrete Fourier transform to obtain the complex wave amplitude at time t_s, $\hat{U}(k\Delta x)|_{t=t_s}$. Solving for Φ in equation (13) and substituting the numerical solution gives the following relationship for the modified wavenumber[2]

$$\Phi(k\Delta x) = \frac{i\Delta x}{at_s}\log\left(\frac{\hat{U}(k\Delta x)|_{t=t_s}}{\hat{U}_0}\right) \tag{14}$$

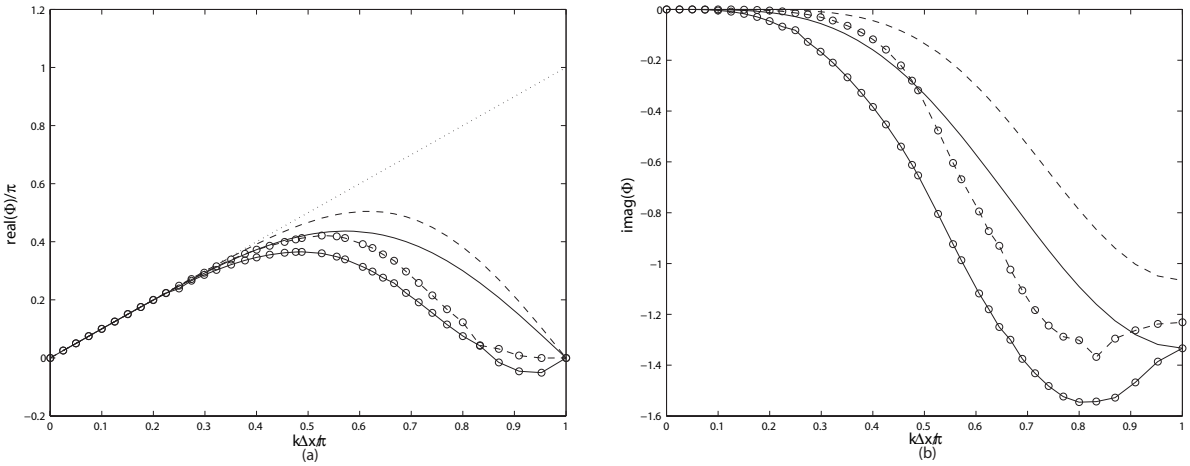

Figure 1. Real (a) and imaginary (b) parts of the modified wavenumber for the the following schemes, — 3rd upwind, — — 5th order upwind, —o 3rd order WENO, — —o 5th order WENO

Following this analysis, the dispersion and dissipation properties of the WENO schemes can be approximately determined. The modified wavenumber is calculated for third and fifth order WENO schemes. To understand the behavior of the nonlinear weights on a linear traveling wave, the modified wavenumber is obtained with and without active substencil smoothness indicators. In smooth regions, WENO is designed to revert to the nominal higher order upwind scheme. The same nominal higher order upwind scheme is achieved by deactivating the nonlinear WENO weights. Figure 1a and 1b depict, respectively, the real part of the modified wavenumber, scaled by π, and the non-scaled imaginary part of Φ versus the reduced wavenumber scaled by π, $k\Delta x/\pi$. Note, third and fifth order upwind curve represent the schemes with deactivated WENO weights, while third and fifth order WENO curves represent the schemes with activated WENO weights. For upwind schemes the typical trends for dispersion and dissipation are obtained. Furthermore, activation of the WENO weights has the effect of making both third and fifth order schemes more dispersive and dissipative than their linear counterparts. That is, more grid resolution is by default necessary when using WENO.

Taking this analysis a step further one can estimate the resolution necessary to simulate a wave traveling a given distance with dissipation below some tolerance. Here, we consider a long-range propagation over 100 wavelengths, which is relevant to our receptivity study. The amplitude decay is obtained by setting the time, t, in the linear model solution (13) to that of a hundred wavelengths of travel, $t = 100\lambda/a$, where $\lambda = 2\pi/k$. Normalizing by the original wave amplitude gives the fractional decay, which is plotted against the reduced wavenumber scaled by π in figure 2. Note that the typically accepted grid resolution of twenty points per wavelength, or $k\Delta x/\pi = 0.1$, is appropriate only for the fifth order upwind scheme, that is, it retains more than 97% of its original amplitude. For the remaining schemes, the amplitude of the propagated wave decays to a value below ninety, thirty and one percent of its original value for the fifth order WENO, third order upwind and the third order WENO schemes, respectively.

Indeed, for fifth order WENO any grid using over approximately thirty points per wavelength would be sufficient, while, for a third order upwind scheme the required grid resolution would need to be seventy to eighty points per wavelength. Last, for the third order WENO scheme, more than one hundred points per wavelength are needed in order to reduce a decay within reason.

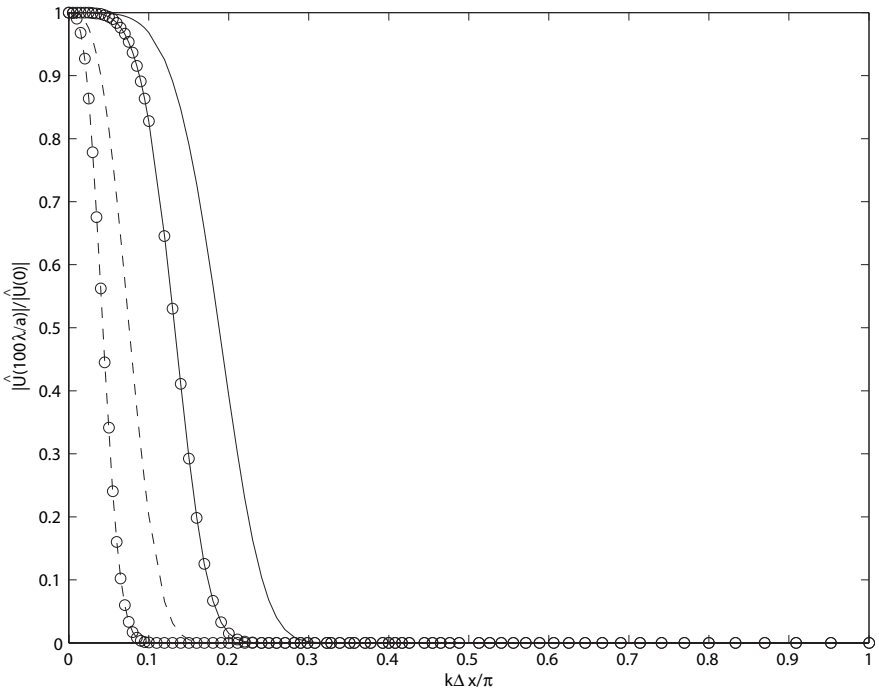

Figure 2. Fractional amplitude decay over a hundred wavelengths for the the following schemes, — — 3rd upwind, — 5th order upwind, — —o 3rd order WENO, —o 5th order WENO

V. Problem statement

The receptivity study is focused on a flat-plate boundary layer under supersonic conditions. An oblique shock develops at the leading edge of the flat plate due to the viscous boundary layer effects. Freestream disturbances must first pass through the oblique shock, generating acoustic, entropy and vorticity waves downstream. These waves diffract at the leading edge and reflect at the flat plate boundary propagating back to the oblique shock, causing further reflections. Since, in a shock capturing scheme, the order of accuracy near the shock reduces to first order, the accurate propagation of freestream disturbance across the shock will be crucial. In this study the freestream parameters are the same as ones used in Ma & Zhong,[21,22]

$$M_\infty = 4.5 \qquad T_\infty = 61.16 \text{ K}$$
$$p_\infty = 728.4381557 \text{ Pa} \qquad Pr = 0.72$$
$$\text{Unit Reynolds number:} \quad Re_\infty = \frac{\rho_\infty u_\infty}{\mu_\infty} = 7.2 \times 10^6 \text{ m}^{-1}$$

The flow field is depicted in figure 3. Ma & Zhong[21,22] solved this problem using a fifth-order shock fitting algorithm. With this approach, they were able to get very close to the leading edge, however, were unable to compute the disturbances at the singular point; instead a TVD scheme was used to generate the shock root. They observed the coexistence of a family of stable boundary layer modes, for example, mode I and mode II, with the unstable second Mack mode. Here, mode I and mode II are generated by the fast acoustic wave commonly referred to as mode F. Although the unstable Mack mode did not directly respond to the freestream disturbance, it interacted through the stable boundary layer modes which acted as an energy exchange medium. Hence, the accuracy of shock capturing schemes will be evaluated on wave propagation through the shock and the exchange of energy between freestream disturbances and boundary layer modes. Furthermore,

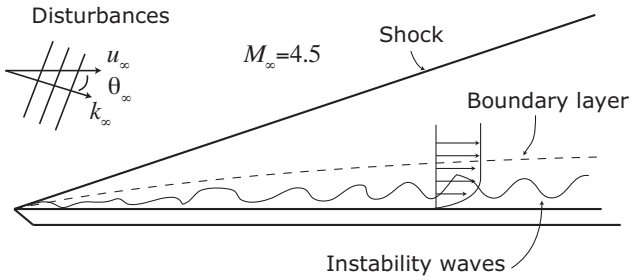

Figure 3. A diagram of the receptivity of a flat plate boundary layer adapted from Ma & Zhong's studies.[21]

effects of the leading edge will be observed, which were previously excluded. In the studies of Ma & Zhong, the forcing was provided by a plane acoustic mode varied over several frequencies and with varying incident angles. We will test one of their cases in this study with a forcing frequency of 177.81 kHz with an amplitude of $\hat{u} = 5 \times 10^{-5} u_\infty$ and an incident angle of zero degrees for a fast acoustic wave and an adiabatic wall boundary condition. For this frequency and flow parameters the resulting wavelength of the fast acoustic mode is approximately 4.8 mm.

VI. Results

A. Grid for the receptivity study

The computational domain roughly starts a third of one wavelength upstream of the leading edge and ends approximately one hundred wavelengths downstream of the leading edge in the streamwise direction, or -0.0018 m $< x <$ 0.5 m. In the wall normal direction, the computational boundary extends from the wall to 0.01 m at the upstream inlet and to 0.136 m at the downstream end. This distribution gives the computational grid a tapered angle of approximately fourteen degrees, roughly tracing the shock present due to the leading edge. For this domain, both the third and fifth order WENO schemes are used to compute the unsteady solutions. As determined previously in section IV, the third order WENO scheme requires approximately one hundred points per wavelength in order to appropriately control dissipation over a domain of one hundred wavelengths. The resolution is kept the same for the fifth order WENO scheme to conduct a grid convergence study. Hence, 10036 points are used in the streamwise direction and 240 points in the wall normal direction. Grid clustering is used in the wall normal direction so that the boundary layer is resolved roughly with thirty to forty points through most of the domain. The freestream forcing has a zero incident angle, and the weak leading edge shock only bends the freestream wave by about a degree.[22] Therefore, a resolution of 240 grid points is sufficient in the wall normal direction. The simulations are run with a CFL number of 0.49. The boundary conditions along the bottom of the computational domain upstream of the leading edge are symmetry conditions, while downstream of it they are adiabatic wall conditions. At the downstream end of the domain, higher order extrapolation is used since most of the flow is in the supersonic regime.

In the previous study with a shock fitting method (Ma & Zhong[22]) the grid consisted of roughly 2470 points in the streamwise and 121 points in the wall normal direction respectively. This resolution disparity is due to two differences. First, the previous study was conducted using a shock fitting method, that is, the leading edge shock was at the upper domain boundary. In this work, the leading edge shock needs to captured, hence twice the number of points in the wall normal direction are used to achieve a sufficient resolution of the shock. Second, the previous study used an optimized low dissipation fifth order upwind scheme, hence they were able to use only seventeen

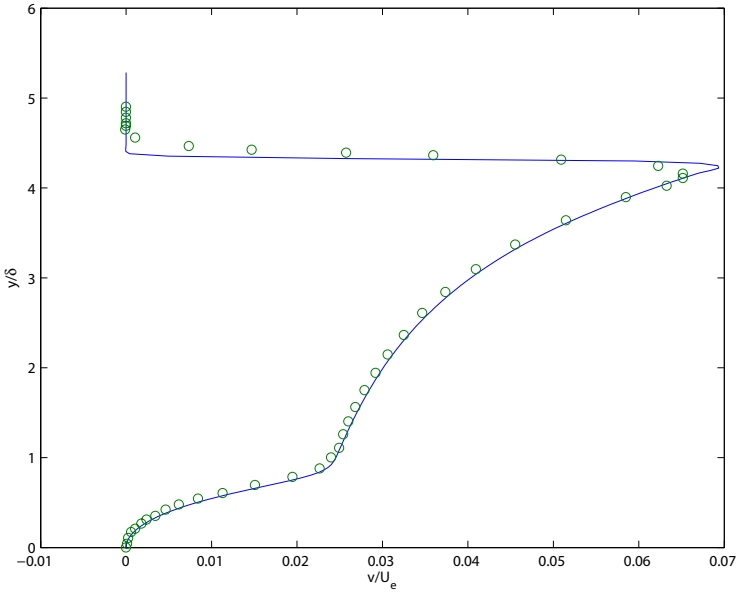

Figure 4. Wall normal velocity comparison at $Re_x = 50400$, blue line 3rd order WENO, current study, green circles TVD steady state solution, previous study of Ma & Zhong.[22]

points per wave in the streamwise direction. It is believed that the grid point increase factor of four in the streamwise direction is only needed for the third order WENO; for the fifth order WENO the previous wavenumber analysis suggests that a coarser grid with approximately 25-30 points per wavelength is sufficient. This will be explored in future work.

B. Third order WENO

The simulation is first run without any freestream forcing to a steady state. The steady state solution agrees well with the previous study of Ma & Zhong[22] as depicted by figure 4, which compares the wall normal velocity profile at $Re_x = 50400$, where Re_x is simply $Re_x = Re_\infty x$. Upon reaching the steady state solution with an acceptable residual tolerance, the freestream forcing is activated. The freestream forcing is applied at the inflow boundary and along the top tapered boundary of the computational domain. Note that the top computational boundary has a positive tapering and this boundary is in the freestream supersonic region, hence most of the information there is flowing into the computational domain. Therefore, it may be considered as another inflow boundary. The additional forcing along the top inflow boundary also aids in countering much of the added dissipation due to the nonlinear WENO weights. A stationary solution is reached by advancing time to roughly 140 wavelengths of travel: one hundred wavelengths to clear the domain and an additional forty to remove any possible remaining numerical transients within the computational domain.

In the previous study of Ma & Zhong,[22] it was shown that a stable boundary layer mode (mode I) is generated by the fast acoustic wave near the leading edge, which is dominant up to $x = 0.1$ m, approximately. There it synchronizes with the second unstable Mack mode, which then is dominant up to x =0.2 m, approximately. Just downstream of $x = 0.2$ m, the fast acoustic wave gives rise to another stable boundary layer mode called mode II, which peaks around $x = 0.3$ m. The third order WENO scheme is able to capture these flow phenomena. The strong initial freestream and mode I interaction can be seen in the instantaneous density perturbation contours near the leading

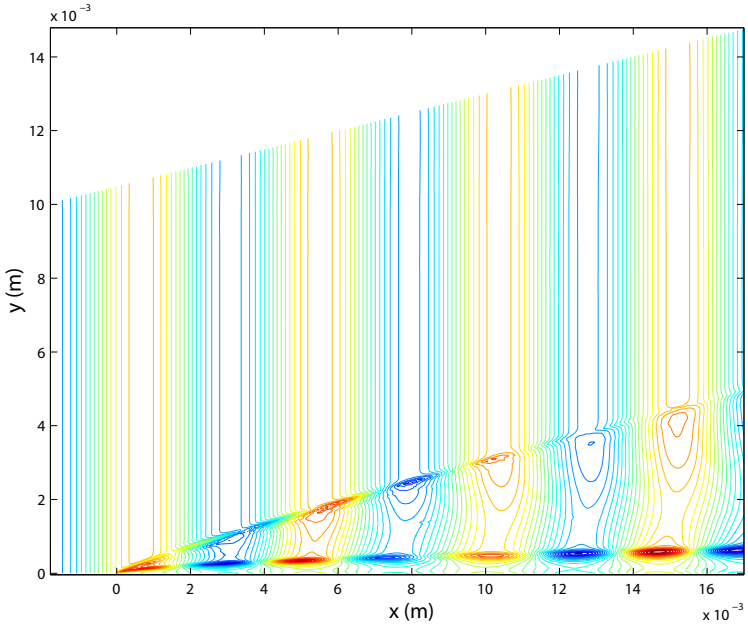

Figure 5. Fluctuating density contours between -0.0018 m $< x < 0.017$ m

edge, as shown in figure 5. The hairpin structure of the second Mack mode is clearly visible in the density contours over the streamwise region of 0.1 m $< x <$ 0.2 m , as shown in figure 6.

In figure 7 the pressure amplitude along the wall is plotted for both the current study and the previous computational study of Ma & Zhong.[22] Over the very fine grid of a hundred points per wavelength, the third order WENO scheme accurately captures the second Mack mode instability associated with the fast acoustic wave. However, differences are present for mode I and mode II when comparing with previous results of Ma & Zhong.[22] The amplitude associated with mode I is much stronger when compared with the Ma & Zhong study, while the amplitude associated with mode II is weaker. The differences with mode I are mainly present due to the difference in the computational domain. That is, in the previous study the leading edge was not part of the computational domain. Furthermore, the freestream forcing is applied through Rankine-Hugoniot jump condition at the shock computational boundary and only there; a freestream forcing could not be applied at the upstream inflow boundary. Hence, the flow very close to the leading edge would be subjected to an initial adjustment region where it would correct itself. That is, the freestream plane wave forcing is not a plane wave everywhere. This is particularly true near the leading edge, where strong freestream and boundary layer mode interaction due to diffusion and diffraction, as predicted by theoretical studies,[39,40] may have been underestimated. The second Mack mode behavior between $x = 0.1$ m and $x = 0.2$ m agrees well with the previous study by Ma & Zhong.[22] The only difference is that the second mode extends well into the region where mode II reaches its peak amplitude. Last, the difference in mode II is possibly due again to the inclusion of the leading edge, which results in a much stronger amplification of the mode I. Mode I takes time to decay, hence it is possible that due to this strong initial amplification the presence of mode I remains significant in the region where mode II peaks and is modifying the flow behavior. A more concrete explanation would be possible after decomposition of these individual modes, which will be pursued in future studies.

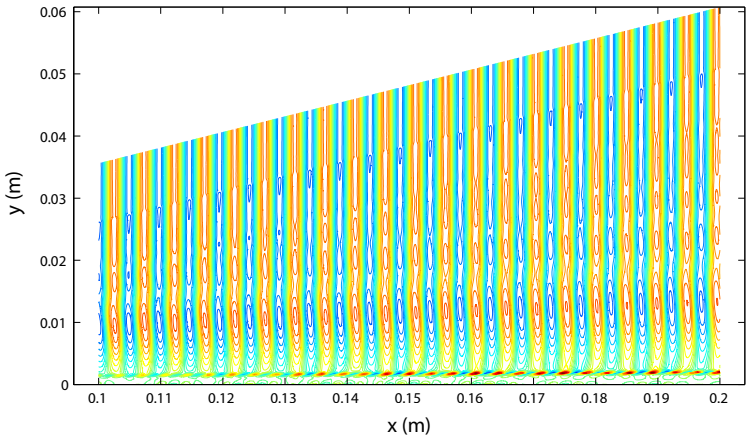

Figure 6. Fluctuating density contours between 0.1 **m** $< x <$ 0.2 **m**

C. Fifth order WENO

The simulation for the fifth order WENO was run on the same grid as the third order study. The fifth order computation was not as straightforward as the third order case, because numerical noise is present in the fluctuating solution downstream of the shock. Due to the linear nature of this problem, it is possible to filter this noise with a discrete Fourier transform in time. The Fourier transform in time is applied over one period. Figure 8a shows the filtered fluctuating density contours for the fifth order WENO scheme, while figure 8b shows the non-filtered fluctuating density contours for the same scheme. Moderate noise is present for the higher order WENO scheme. This issue will be further explored in future studies.

VII. Conclusion

In the present work, two shock capturing algorithms, third order and fifth order WENO, were compared to a previous study of a supersonic boundary layer over a flat plate. It was found that the third order WENO scheme is very dissipative over the domain of interest and that a grid of one hundred points per wavelength was needed to counter its dissipation. For the third order WENO scheme, a good agreement was obtained for the second Mack mode instability, however differences were noted for mode I and mode II. These difference are most likely due to the inclusion of the leading edge, which in the previous study was excluded due to algorithm limitations. A more in depth analysis will be conducted to understand these difference in future studies. Fifth order WENO is not as dissipative according to the frequency analysis, and 25-30 points per wavelength are sufficient for the current study. However the fifth order WENO solution has numerical noise downstream of the shock. This is a subject of ongoing research and we hope to answer some of these questions in future studies.

VIII. Acknowledgments

The authors gratefully acknowledge support by the NASA Fundamental Aeronautics Program, under cooperative agreement NNX07AC39A, monitored by Dr. Meelan Choudhari.

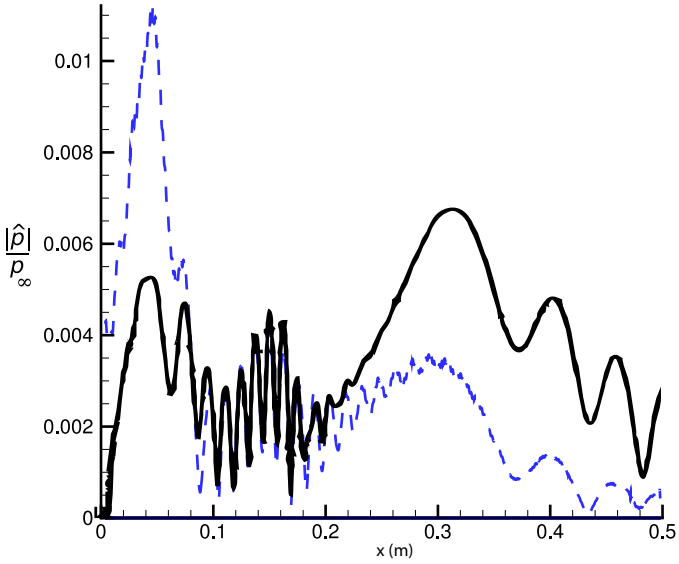

Figure 7. Pressure amplitude along the wall normalized by the freestream pressure, p_∞, dashed blue line 3rd order WENO, current study, solid black line fifth order shock fitting, previous study of Ma & Zhong[22]

References

[1]S.K. Lele. Compact finite-difference schemes with spectral-like resolution. *Journal of Computational Physics*, 103:1:16–42, 1992.

[2]S. Pirozzoli. On the spectral properties of shock-capturing schemes. *Journal of Computational Physics*, 219:2:489–497, 2006.

[3]J.C. Tannehill, D.A. Anderson, and R.H. Pletcher. Computational fluid mechanics and heat transfer. *Taylor and Francis*, 2nd ed, Washington DC, 1997

[4]C. Hirsch Numerical Computation of Internal and External Flows. *Wiley*, New York, 1988

[5]Th. Herbert, and M.V. Morkovin. Dialogue on progress and issues in stability and transition research. In *Laminar-Turbulent Transition, IUTAM Symp. Stuttgart, Germany* (ed. R. Eppler & H. Fasel), Springer, 47–72, 1979

[6]M.V. Morkovin, and E. Reshotko. Dialogue on progress and issues in stability and transition research. In *Laminar-Turbulent Transition, IUTAM Symp. Toulouse, France* (ed. D. Arnal & R. Michel), Springer, 1989

[7]J.F. Mckenzie, and K.O. Westpal. Interaction of Linear Waves with Oblique Shock Waves. *Physics of Fluids*, 11:11:2350–2362, 1968.

[8]I.V. Egorov, A.V. Fedorov, and V.G. Soudakov Direct Numerical Simulation of Unstable Disturbances in Supersonic Boundary Layer. *AIAA* 2004–0588, 2004.

[9]E. Reshotko. Is Re_θ/Me a meaningful transition criterion ? *AIAA* 2007–0943, 2007.

[10]M.V. Morkovin, E. Reshotko, and T. Herbert. Transition in open flow systems - a reassessment. *Bulletin of the American Physical Society*, 39:1882, 1994.

[11]F.P.Bertolotti. Vortex generation and wave-vortex interaction over a concave plate with roughness and sction. *ICASE Report*, 93–101, 1993.

[12]E. Reshotko. Transient growth: A factor in bypass transition. *Physics of Fluids*, 12:5:1067-1075, 2001.

[13]A. Tumin, X. Wang, and X. Zhong. Direct numerical simlation and the theory of receptivity in a hypersonic boundary layer. *Physics of Fluids*, Vol. 19, Paper No. 014101, 2007.

[14]E.B. White, J.M. Rice, and F.G. Ergin. Receptivity of stationary transient disturbances to surface roughness. *Physics of Fluids*, Vol. 17, No. 6, Paper No. 064109, 2005.

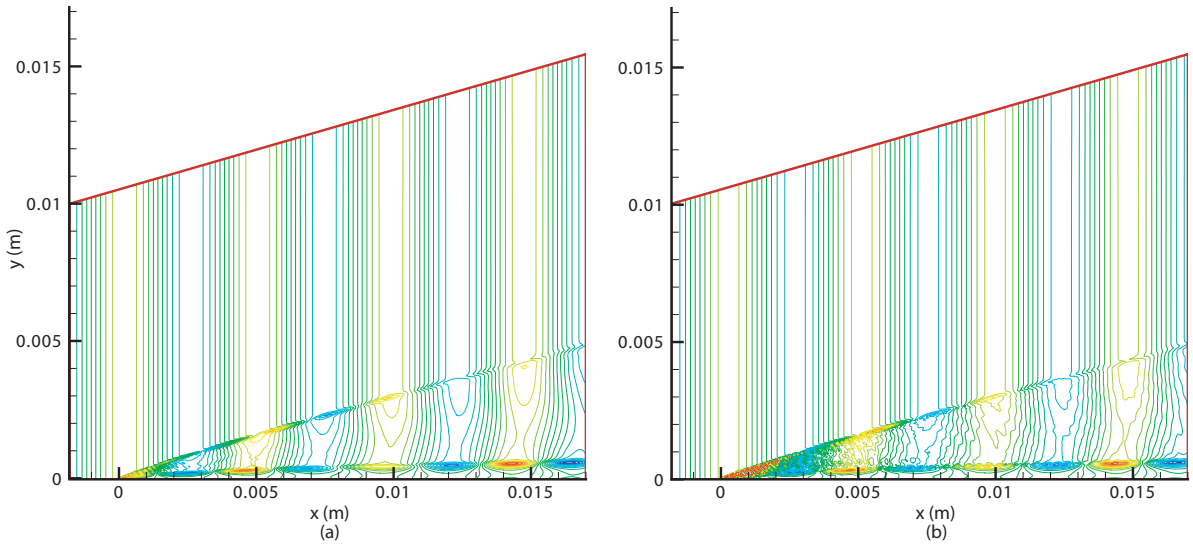

Figure 8. Fluctuating density contours near the leading edge computed using the fifth order WENO scheme, (a) FFT filtered results, (b) non-filtered results

[15]M.R. Malik. Hypersonic boundary-layer receptivity and stability. In *Laminar-Turbulent Transition, IUTAM Symp.* (ed. H.F. Fasel & W.S. Saric), Springer, 407–414, 2002

[16]R. Lin, M.R. Malik, and R. Sengupta. Computation of hypersonic boundary-layer response to external disturbances *AIAA paper* 1999–0411, 1999.

[17]E.J. Kerschen. Boundary-layer receptivity. *AIAA paper* 1989–1109, 1989.

[18]E. Reshotko. Boundary layer instability, transition and control. *AIAA paper* 1994–0001, 1994.

[19]E. Reshotko. Environment and receptivity. *AGARD Rep.*, 709, 1984.

[20]Th. Herbert. Progress in applied transition analysis *AIAA paper* 1996–1993, 1996.

[21]Y. Ma, and X. Zhong. Receptivity of a supersonic boundary layer over a flat plate. Part 1. Wave structures and interactions. *Journal of Fluid Mechanics*, 488:31–78, 2003a.

[22]Y. Ma, and X. Zhong. Receptivity of a supersonic boundary layer over a flat plate. Part 2. Receptivity to free-stream sound. *Journal of Fluid Mechanics*, 488:79–121, 2003b.

[23]Y. Ma, and X. Zhong. High-order finite-difference schemes for numerical simulation of hypersonic boundary-layer transition. *Journal of Computational Physics*, 144:662–709, 1998.

[24]C.W. Shu, and S. Osher. Efficient implementation of essentially non-oscillatory shock-capturing schemes, ii. *Journal of Computational Physics*, 83:32–78, 1989.

[25]S. Pirozzoli Conservative hybrid compact-weno schemes for shock-turbulence interaction. *Journal of Computational Physics*, 178:81–117, 2002.

[26]D.J. Hill, and D.I. Pullin. Hybrid tuned center-difference-WENO method for large-eddy simulation in the presence of strong shocks. *Journal of Computational Physics*, 194:435–450, 2004.

[27]Y.X. Ren, M. Liu, and H. Zhang A characteristic-wise compact-WENO scheme for solving hyperbolic conservation laws. *Journal of Computational Physics*, 192:365–386, 2003.

[28]M.P. Martín, E.M. Taylor, M. Wu, and V.G. Weirs. A bandwidth-optimized WENO scheme for the effective direct numerical simulation of compressible turbulence. *Journal of Computational Physics*, 220:270–289, 2006.

[29]E.M. Taylor, M. Wu, and M.P. Martín. Optimization of nonlinear error for weighted essentially non-oscillatory methods in direct numerical simulations of compressible turbulence. *Journal of Computational Physics*, 223:384–397, 2007.

[30]D.S. Balsara, C. Altmann, C. Munz A sub-cell based indicator for troubled zones in RKDG schemes and a novel class of hybrid RKDG+HWENO schemes. *Journal of Computational Physics*, 226:586–620, 2007.

[31]G.S. Jaing, and C.W. Shu. Efficient implementation of weighted ENO schemes. *Journal of Computational Physics*, 126(1):202–228, 1996.

[32]X. Zhong. Leading-edge receptivity to freestream disturbance waves for hypersonic flow over a parabola. *Journal of Fluid Mechanics*, 441:315–367, 2001.

[33]J.M. Kendall. Wind tunnel experiments relating to supersonic and hypersonic boundary-layer transition *AIAA Journal*, 13:290–299, 1975.

[34]L.M. Mack. Linear stability theory and the problem of supersonic boundary-layer transition *AIAA Journal*, 13:278–289, 1975.

[35]S.R. Pate. Measurements and correlation of transition Reynolds number on sharp slender cones at high speeds. *AIAA Journal*, 9:1082, 1971.

[36]S.R. Pate, and C.J. Schueler. Radiated aerodynamic noise effects on boundary-layer transition in supersonic and hypersonic wind tunnels. *AIAA Journal*, 7:450, 1969.

[37]L.M. Mack. Boundary layer linear stability theory. *AGARD Rep*, 709, 1984.

[38]A.A. Maslov, and N.V. Semionov. Excitation of nature oscillations in a boundary layer. *Fluid Dyn.*, 3:74–78, 1986

[39]A.V. Fedorov, and A.P. Khokhlov. Excitation of unstable modes in a supersonic boundary layer by acoustic waves *Fluid Dyn.*, 4:67–74, 1991

[40]A.V. Fedorov, and A.P. Khokhlov. Sensitivity of a supersonic boundary layer to acoustic disturbances *Fluid Dyn.*, 1:40–47, 1992.

[41]A.V. Fedorov, and A.P. Khokhlov. Prehistory of instability in a hypersonic boundary layer. *Theoret. Comput. Fluid Dyn.*, 14:359–375, 2001.

[42]A.V. Fedorov, and A.P. Khokhlov. Receptivity of hypersonic boundary layer to wall disturbances. *Theoret. Comput. Fluid Dyn.*, 15:231–254, 2002.

[43]A.V. Fedorov, and A. Tumin. Initial-value problem for hypersonic boundary layer flows. *AIAA paper* 2001–2780, 2001.

[44]K.F. Stetson, and R.L. Kimmel On hypersonic boundary layer stability *AIAA paper* 1992–0737, 1992.

[45]K.F. Stetson, E.R. Thompson, J.C. Donaldson, and L.G. Siler. Laminar boundary layer stability experiments on a cone at Mach 8, Part 4: on unit Reynolds number and environmental effects. *AIAA paper* 1986–1087, 1986.

[46]J. Casper, and M.H. Carpenter. Computational considerations for the simulation of shock-induced sound. *SIAM J. Sci. Comput.*, 19:813, 1998

[47]A.A. Maslov, A.N. Shiplyuk, A. Sidorenko, and D. Arnal Leading-edge receptivity of a hypersonic boundary layer on a flat-plate. *Journal of Fluid Mechanics*, 171:219-261, 2001.

[48]J.L. Potter, and J.D. Whitfield Effects of slight nose bluntness and roughness on boundary layer transition in supersonic flow. *Journal of Fluid Mechanics*, 12:501–535, 1969.

[49]W.S. Saric, H.L. Reed, and E.J. Kerschen. Boundary-layer receptivity to free-stream disturbances *Annu. Rev. Fluid Mech.*, 34:291–319, 2002.

[50]M.E. Goldstein, and L.S. Hultgren. Boundary-layer receptivity to long-wave free-stream disturbances. *Annu. Rev. Fluid Mech.*, 21:137–166, 1989.

[51]X.D. Liu, S. Osher, and T. Chan Weighted Essentially Non-oscillatory Schemes. *Journal of Computational Physics*, 115:200–212, 1994.

[52]S. Candel, D. Durox, and T. Schuller. Efficient Implementation of Essentially Non-oscillatory Shock-Capturing Schemes, II. *Journal of Computational Physics*, 83:37–78, 1989.